SPACE-VECTOR PWM VOLTAGE CONTROL WITH OPTIMIZED SWITCHING STRATEGY

Victor R. Stefanovic* and Slobodan N. Vukosavic

(*) Casa EA, Lotto 7C, Pianbosco, 21040 Venegono Superiore, VA, Italy

Abstract: **Space vector modulation in voltage source inverters offers improved DC-bus utilization and reduced commutation losses, and has been therefore recognized as the preferred PWM method, especially in the case of digital implementation. Three-phase inverter voltage control by space vector modulation consists of switching between the two active and one zero voltage vector in such a way that the time average within each switching cycle corresponds to the voltage command. However, the switching sequence is not unique. This paper demonstrates that the sequence most favored in the literature is not the best one over the entire motor speed range. Rather, a preferred switching sequence is defined in the paper as a function of the modulation index and a power factor. The sequence is selected by using the inverter switching losses and the current ripple as the criteria. Results presented in the paper are based on analytical study and are corroborated by experimental data.**

1. INTRODUCTION

Modern AC drives with gate-commutated switches use various PWM methods for voltage or current control. The desirability of a given method depends on:

- -harmonic distortion of the output waveform for a given switching frequency.
- -utilization of a DC bus voltage.
- -dynamic response.
- -ease of implementation.

TABLE I:
DEFINITION OF THE VOLTAGE VECTORS AVAILABLE AT THE INVERTER OUTPUT, THEIR α AND β COMPONENTS AND THE INVERTER SWITCHING STATES.

VECTOR	ANGLE	U_α	U_β	STATES (*) 1 = HIGH 0 = LOW A	B	C	$\lvert\vec{U}_{\alpha\beta}\rvert$
$\vec{V}_1$	0^o	E	0	1	0	0	E
$\vec{V}_2$	60^o	$\frac{E}{2}$	$\frac{E}{2}\sqrt{3}$	1	1	0	E
$\vec{V}_3$	120^o	$-\frac{E}{2}$	$\frac{E}{2}\sqrt{3}$	0	1	0	E
$\vec{V}_4$	180^o	$-E$	0	0	1	1	E
$\vec{V}_5$	240^o	$-\frac{E}{2}$	$\frac{-E}{2}\sqrt{3}$	0	0	1	E
$\vec{V}_6$	300^o	$\frac{E}{2}$	$\frac{-E}{2}\sqrt{3}$	1	0	1	E
$\vec{V}_7$	-	0	0	1	1	1	0
$\vec{V}_8$	-	0	0	0	0	0	0

(*) A,B,C: THE INVERTER LEGS SWITCHING STATES

0-7803-0634-1/92$03.00 ©IEEE

The most preferred PWM technique today is space vector modulation [1],[2],[4] which offers 15% better bus utilization and 33% fewer commutations per cycle than conventional PWM. While some other methods (as, for example, the one proposed by Ziogas et al [6]) give the same results, space vector modulation is better suited for digital implementation.

In each cycle of space vector modulation, the desired output voltage is approximated by a time average of three voltage vectors (three switching states). Of these, two are non-zero voltage vectors adjacent to the reference (for example, vectors 1 and 2 are adjacent to the reference vector in Fig. 1), while the third one is a zero vector. The strategy of sequencing these three switching states within each cycle will influence the current ripple, the commutation losses and the spectrum of the output voltages and currents.

Basically, there are two practical sequencing possibilities:

The first one [3] uses state 7 (111) as the zero vector in sectors 1, 3, and 5 (Fig.1), and state 8 (000) as the zero vector in sectors 2, 4, and 6. The switching sequence remains the same during switching in the same sector (Fig. 2). For example, for reference in the first sector, Fig.1, the sequence is 100-110-111-100-110-111, etc. This strategy requires four commutations per one switching cycle. In this paper, this strategy is called direct-direct (DD) sequence.

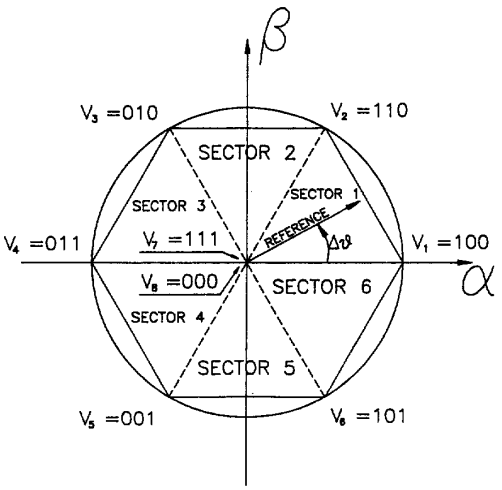

Fig. 1: Location of the inverter vectors $\vec{V}_1..\vec{V}_8$ in the α-β stationary frame (The switching states are defined in Table 1.)

The second one, proposed by many authors [3],[4] and favored today, consists of using the redundancy of zero vectors (states 7 and 8) to reduce the number of commutations per switching cycle. The switching sequence is reversed after passing through each zero vector. For example, for reference in the first sector, Fig. 1, the switching sequence is 100-110-111-110-100-000, Fig. 3. The main advantage of this approach is that it requires only three commutations per cycle and gives symmetrical pulses [5]. This strategy is called here a direct-inverse (DI) sequence.

Since the space vector modulation offers superior performance with respect to other modulation techniques, it is important to establish the sequencing strategy which is best suited for variable frequency AC drives. This paper presents analytical and experimental results in order to compare these two strategies and outline their most important characteristics. In Section 2, both sequencing strategies are defined, and for each of them analytical expressions are derived for the RMS value of the current ripple as a function of the modulation index. Section 3 presents experimental data which consist of the stator current waveforms of an induction motor, their spectra, and the RMS values of the ripple current for both sequencing strategies. The experimental results, obtained for output voltages from 0.2 to 1.0 p.u., confirm those derived analytically.

The discussion in Section 4 summarizes the characteristics of reversing (DI) and non-reversing (DD) sequences, and clearly shows that a reduction in the number of commutations obtained with DI sequence does not result in a corresponding reduction of the commutation losses for the most important class of inverter loads (motor drives and UPS' under rated load). For that case, the paper recommends the DD sequence. For other cases, the paper shows that the best results are obtained by using DI sequence for low output voltage and DD sequence when the modulation index is increased. Section 5 gives some concluding remarks, while the two Appendices present the details of the performed calculations.

2. ANALYTICAL CONSIDERATIONS

2.1 Review of space vector modulation

A three-phase inverter can assume 8 different switching states, corresponding to 7 discrete voltage vectors at the output (Fig.1). The PWM strategy defines the sequencing of the available vectors in such a way that the average voltage within one cycle corresponds to the reference $\vec{U}^*$. The cycle time T is defined as the time necessary to go through the sequence of three successive vectors (interval T in Figs. 2 and 3). The cycle T can also be defined as the minimum interval where the average inverter output corresponds to the reference $\vec{U}^*$.

The space vector modulation and the problem of selecting the appropriate switching sequence is best understood if the phase quantities are transformed into the α-β stationary reference frame:

$$u_\alpha = u_a - \frac{u_b+u_c}{2}\ ,\ u_\beta = -\frac{\sqrt{3}}{2}(u_b+u_c) \qquad (1)$$

(u_a, u_b, and u_c are the phase voltages, u_α and u_β are the components of the voltage vector $\vec{u}_{\alpha\beta}$, axes α is aligned with the motor phase A winding).

Table I gives the α and β components of each voltage vector, together with the switching states for all six segments defined in Fig. 1. (E denotes the DC-bus voltage).

The non-zero vectors $\vec{V}_1..\vec{V}_6$ create a hexagon Fig.1 centered in the origin of the α-β plane, with the internal diameter $d = E\sin(60^\circ)$ and the external diameter $D = E$. The zero voltage vectors are located in the origin of the α-β plain ($\vec{V}_7$= 111 and $\vec{V}_8$= 000) and they both short circuit the load.

Any reference vector $\vec{U}^*$ located inside the hexagon, Fig. 1, can be realized within one switching cycle T as a time average of three voltage vectors. The maximum non-distorted output which can be obtained is when the vector $\vec{U}_{\alpha\beta}$ tracks the circular locus inscribed into the hexagon (Fig.1); $|\vec{U}_{\alpha\beta}|_{max} = E\sin(60^\circ)$. That voltage represents the physical limit obtainable without distortion and is 15.4% higher than the maximum voltage obtained with sinusoidal modulation. It also represents 90.6% of the fundamental voltage obtained with a six-step modulation [3],[4]. Referring to Fig. 1, it is impossible to reach all the points on the circle that is circumscribed around the hexagon. Moreover, the modulation can be arranged in such a way that the output voltage $\vec{U}_{\alpha\beta}$ tracks the hexagon boundaries, but then the voltage components U_α and U_β (as well as line-to-line voltages U_{ab}, U_{bc}, and U_{ca}) will be non-sinusoidal.

The best tracking of the reference voltage $\vec{U}^*$ is obtained when the switching sequence includes only the two vectors adjacent to $\vec{U}^*$ and a zero vector [3],[4]. The aim of this paper is to derive the optimum sequencing of these three vectors, with respect to the ripple current and the commutation losses.

The time intervals T_1, T_2, and T_o (Fig.2), determine the duration of the three vectors that compose the switching sequence. These intervals depend on the amplitude and the spatial orientation of the reference vector $\vec{U}^*$. Assume first that the reference $\vec{U}^*$ is in sector 1, Fig.1 and that it has an amplitude A and the angle $\theta = \arg(\vec{U}^*)$ with respect to the α axes. The two adjacent non-zero voltage vectors are $\vec{V}_1$ and $\vec{V}_2$. Notice in Fig.1 that the displacement between the reference $\vec{U}^*$ and the clockwise-side vector $\vec{V}_1$ is $\Delta\theta = \arg(\vec{U}^*) - \arg(\vec{V}_1^*)$. Define the modulation index $m = A/d$, where $d = E \sin(60^\circ)$ and represents the radius of the circle inscribed in the hexagon. The intervals T_1, T_2, and T_o are given by expressions (2-3):

the vector $\vec{V}_1$ is applied during the interval

$$T_1 = T\, m \sin(60^\circ - \Delta\theta), \quad (2),$$

the vector $\vec{V}_2$ is applied during the interval

$$T_2 = T\, m \sin(\Delta\theta), \quad (3),$$

and the zero vector is applied during

$$T_o = T - T_1 - T_2.$$

The same rule (2-3) defines the intervals T_n, T_{n+1}, and T_o for any other sector in the hexagon. Depending on the spatial orientation of the voltage reference $\vec{U}^*$, each modulation cycle should consist of the sequence of vectors $\vec{V}_n$, $\vec{V}_{n+1}$, and $\vec{V}_{7/8}$, where $n \in [1..6]$ is the sector number, while the angle $\Delta\theta$ is $\arg(\vec{U}^*) - (n-1)\times 60^\circ$. The zero vector is applied to the inverter output during the interval $T_o = T - T_1 - T_2$ in each cycle.

2.2 Regular sequencing strategy

With this strategy, the switching sequence is repeated in each cycle as long as the reference vector is within the same sector. For the case when a reference is in sector 1, the switching sequence is given in Fig.2. If $\vec{V}_7$ is selected as the zero vector, each switching cycle will have two commutations in the inverter leg B and two in leg C (a total of 4), while leg A will have the upper switch ON during the entire cycle. If the zero vector is $\vec{V}_8$ (000), the number of commutations (i.e. transitions) per cycle will be the same, but the inverter leg that will cease commutating in sector 1 will be leg C.

This redundancy of zero vectors allows for a reduction of commutation losses. Selection of the zero vector should be done so as to avoid commutation in the inverter leg carrying the largest current. Assuming a case of an induction motor with the inverter output current lagging the reference $\vec{U}^*$, one can conclude that within the sector 1 the current i_a reaches its peak, while the current i_c crosses the zero. Therefore, reduced commutation losses can be expected if vector $\vec{V}_7$ (111) is selected as the zero vector for the sector 1. Following the same rule, vector $\vec{V}_7$ should be also selected in sectors 3 and 5, while $\vec{V}_8$ should be used in sectors 2, 4, and 6, Fig.1. As a consequence, inverter leg A will not commutate in sectors 1 and 4 (Fig.1); leg B in sectors 3 and 6, while inverter leg C will not commutate when the reference vector lies in sectors 2 and 5. Hence, for the sequencing strategy illustrated in Fig. 2, each inverter leg will not commutate for $2\times 60^\circ = 120^\circ$ within each period of the fundamental.

Considering the number of commutations of the inverter legs per time unit, the switching cycle $T = 1/f_c$ of the space vector modulation with regular (DD) sequencing can be related to the chopping frequency f_{PWM} (or, the carrier period $T_{PWM} = 1/f_{PWM}$) of the sinusoidal carrier-based PWM. For the same number of inverter switchings, the relation is $T_{PWM} = 1.5\, T$ (or, $f_{PWM} = 2/3\, f_c$).

2.3 Reverse sequencing strategy

One can modify the switching sequence between the three voltage vectors so that each transfer from one to the other state involves only one commutation [3],[4], Fig.3. This obviously requires the use of both zero vectors ($\vec{V}_7$ and $\vec{V}_8$) in a given sector and a reversal of the switching sequence every cycle. The benefit is a reduction of commutations from four (obtained with a regular sequence) to three (compare the number of commutations in Figs. 2 and 3). The space vector modulation with the inversed (DI) sequence and the cycle frequency $f_c = 1/T$ has the same number of inverter switchings as the sinusoidal PWM with the carrier frequency $f_{PWM} = f_c/2$.

2.4 Analytical comparison

In addition to the number of commutations per switching cycle, the comparison of the DD and DI sequencing strategies requires an

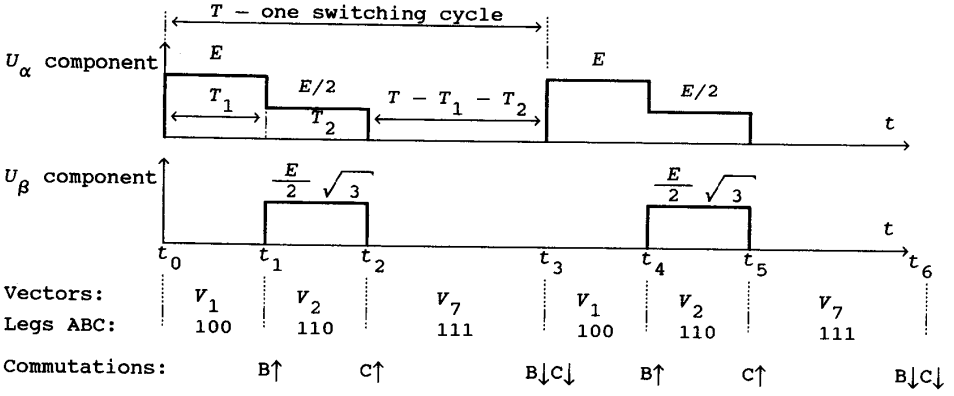

Fig. 2: Timing diagram for space vector modulation with regular (DD) switching sequence and a reference vector in sector 1.

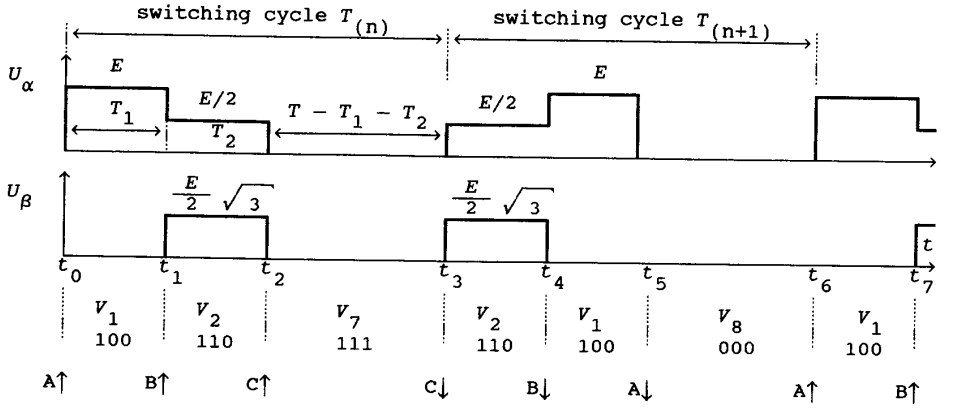

Fig. 3: Timing diagram for space vector modulation with reversed (DI) switching sequence and a reference vector in sector 1.

evaluation of the motor current spectrum and the ripple. The spectrum of the motor current is obtained experimentally for both DD and DI strategies, and is shown in the next section. The ripple is the largest when the reference vector is equidistant from the two adjacent voltage vectors ($\Delta\theta = 30^{\circ}$), so that all analytical expressions for the RMS value of the motor current ripple are derived for that condition in Appendix 1 for both DD and DI strategies. These expressions are:

$$\text{DD: } \Delta i^2_{\alpha\beta rms} = \left(\frac{mTE}{2L_\sigma}\right)^2 \left(\frac{1}{4} - \frac{5}{12}m + \frac{3}{16}m^2\right) \quad (4)$$

$$\text{DI: } \Delta i^2_{\alpha\beta rms} = \left(\frac{mTE}{2L_\sigma}\right)^2 \left(\frac{1}{4} - \frac{5}{12}m + \frac{1}{4}m^2\right) \quad (5)$$

where m is a modulation index, E is a DC-bus voltage, T is the cycle period, and L_σ is the motor equivalent leakage inductance.

Analytical results are illustrated in Fig.4. If both DD and DI strategies have the same switching cycle T, the DI approach will have 25% fewer commutations but will have an increasingly larger ripple than the DD sequence for $m > 0.28$. That is the price for reducing the number of commutations; for $m = 1$ the DI sequence produces twice as large ripple as the DD sequence.

Trace C in Fig.4 corresponds to the DI sequence with a reduced cycle time, $T' = 0.75\ T$, thus having the same commutation frequency as the DD sequence, trace A. The traces in Fig.4 suggest that the best result is obtained by combining these two strategies when operating over the full voltage range. Using only the current ripple and the number of commutations as a criterion, the switch-over point M corresponds to the modulation index of $m = 0.75$, above which one should use DD sequencing strategy. However it is shown in section 4 that this is not the correct choice if switching losses need to be minimized in a typical AC motor drive.

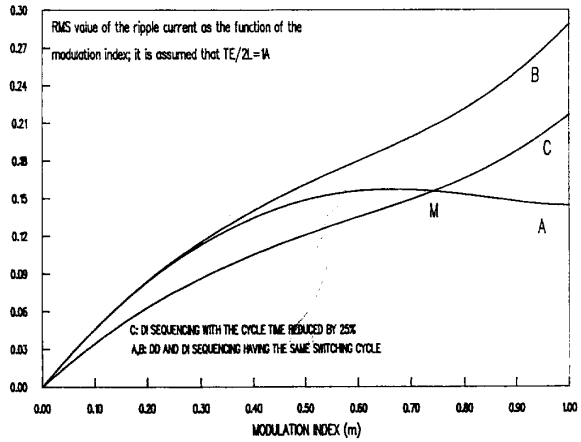

Fig. 4: The RMS value of the current ripple as a function of the modulation index m obtained from equations (4) and (5) with the assumption (TE)/(2Lσ) = 1A. Trace A: with DD sequence; trace B: with DI sequence. Trace C: DI sequence with reduced cycle time; T'= 0.75 T (the same commutation frequency as DD sequence, trace A).

3. EXPERIMENTAL RESULTS

Analytical results given in Section 2 are experimentally verified on a prototype induction motor drive. Parameters of the motor under the test are given in Table II.

TABLE II:
THE PARAMETERS OF THE MOTOR UNDER THE TEST

Motor type: ZK132, 4-pole,		
D-connected standard induction motor		
Rated power (kW):	P	= 7.5 kW
Rated voltage:	U	= 3x380 V, f = 50Hz
Rated current:	I	= 16 A
Stator resistance:	R_s	= 0.038 p.u.
Rotor resistance:	R_r	= 0.043 p.u.
Winding inductances	L_s	= L_r = 1.993 p.u.
Magnetizing inductance:	M	= 1.91 p.u.
Equivalent leakage inductance:	$L\sigma$	= 0.164 p.u.

The induction motor is supplied from a conventional three-phase inverter with IGBT transistors. The motor is controlled in the open-loop, maintaining U/f = const. The motor current is always kept at the rated level, I = 16 A RMS, by adjusting the DC generator load connected to the shaft. A set of experiments is performed, using both DD and DI modulation techniques and sweeping the fundamental frequency from 10Hz to 50Hz. The space-vector modulator (capable of generating both DD and DI patterns) is implemented by using a PC computer and the dedicated hardware illustrated in Fig. 5.

Programming of the PAL is given by the equations (6-8). The PAL inputs ABC determine a sector $n \in [1..6]$ (see Fig.1). Each binary value of ABC from 001 to 110 corresponds to one of the sectors. The values ABC = 000 and ABC = 111 produce a three-phase output RST = 000 and RST = 111 (respectively) independently of the other inputs (D,E,F). The states ABC=111 and ABC=000 are used to maintain the appropriate zero vector and eliminate glitches at the RST outputs at the beginning of each cycle. These glitches could appear due to the fact that the code DABC setting and the 8253 timer reload cannot occur at the same instant.

The input D determines the sequencing strategy: D = 0 gives a DD sequence (Fig. 2). In order to achieve a DI sequence (Fig. 3), the input D is toggled at the beginning of each cycle (D = 1 for the $V2$-$V1$-$V8$ cycle, and D = 0 for $V1$-$V2$-$V7$ cycle; Fig. 3). In such a way, a smooth transition between DD and DI sequencing can be done on-line, simply by changing the logic level of the PAL input D.

The inputs E and F determine the intervals $T1$ and $T2$ of the active (non-zero) voltage vectors. The programmable timer 8253 is reloaded and restarted each 250 μs. The data loaded in counters #1 and #2 are determined in such a way that the output OUT1 ($\bar{E}$) is low during the interval $T1$ (Fig. 2, Eq. 2), while the output OUT2 is low during the period $T1$+$T2$ (from $t0$ to $t2$ in Figs. 2 and 3).

$$R=AB\bar{D}+ABDE+CD\bar{E}\bar{F}+\bar{A}\bar{B}CF+\bar{A}B\bar{C}(DE+\bar{D}\bar{E})+\bar{D}\bar{F}A\bar{B}\bar{C}+\bar{B}CD\bar{E}+ABF$$

$$S=ABC+D\bar{E}\bar{F}C+\bar{A}BF+\bar{A}\bar{B}CD\bar{E}+\bar{A}C\bar{D}E+\bar{A}B\bar{C}\bar{D}+A\bar{B}\bar{C}(DE+\bar{D}\bar{E})+AB\bar{D}\bar{E}\bar{F}$$

$$T=ABC+D\bar{E}\bar{F}C+D\bar{F}B\bar{C}+A\bar{B}F+A\bar{C}(DE+\bar{D}\bar{E})+\bar{A}BC(D\bar{E}+\bar{D}E) \qquad (6),(7),(8)$$

Data loaded in counters and the code DABC are calculated off-line and stored in the appropriate table. Thus, the only task of the real-time software is to read the table and perform the I/O functions. Since the main objective of the experiment was to compare the current ripples of DD and DI sequencing strategies, attention was paid to reduce the influence of the other parasitic current components on the resulting THD (total harmonic distortion). The dead-time was reduced to the minimum (1.5μs) and was adjusted to the same value in all IGBT drivers. The off-line calculation of PWM pattern included the dead-time compensation, assuming that the current lags 30° with respect to the voltage (that is, the current ia is positive in sectors 6,1, and 2. In this way, the influence of the dead-time on the current waveform and THD is significantly reduced.

The recorded phase current for the rated motor current and f = 25Hz (m = 0.5) is shown in Fig. 6 (for DD sequence) and Fig. 7 (for DI sequence). Figs. 8 and 9 present the phase current waveforms for f = 50Hz (m = 1). It can be seen that the difference between the DD and DI sequencing is negligible for m = 0.5. On the other hand, at the rated speed (m = 1, Figs. 8 and 9) the DI sequencing results in a significantly larger current ripple.

The spectra of the waveforms in Figs. 6-9 are obtained numerically and are given in Figs. 10-13. For m = 0.5, the phase current spectrum for the DD (Fig.10) strategy has a predominant component at the cycle frequency of 4 kHz. For m = 0.5 (Fig. 11), the DI spectrum contains the main component at cycle frequency (essentially the same as the one of a DD sequence), and a relatively small component at $f_c/2$ (2kHz).

At rated speed and m = 1, Figs. 12 and 13, the main ripple component with a DI strategy (Fig. 13) is located at half the cycle frequency and has twice the amplitude as that of the DD strategy, Fig.12.

Analytical expressions (Eq. 4, 5; Fig. 4) for the ripple as a function of the modulation

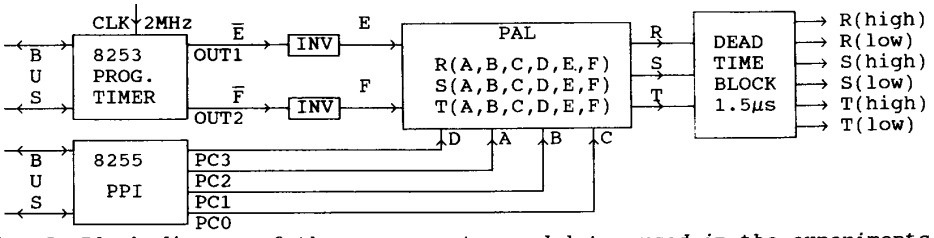

Fig. 5: Block diagram of the space vector modulator used in the experiments

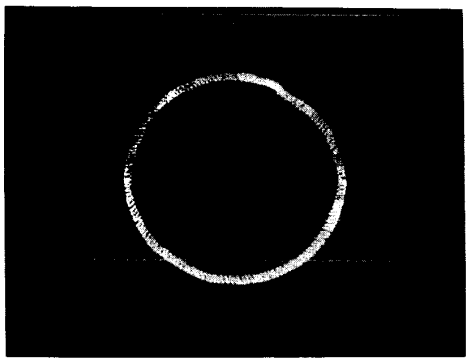

Fig. 6: Motor phase current, 10A/div, $I_{rms}=I_n$, f=25Hz, m=0.5, DD sequence; corresponding vector rotation in α-β plane.

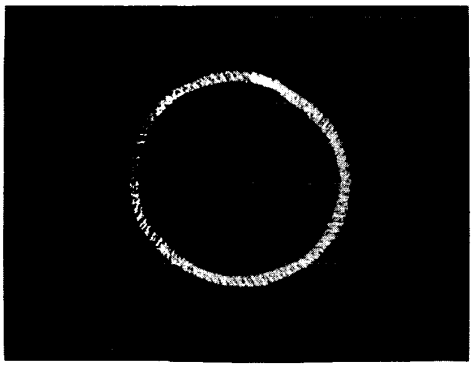

Fig. 7: Motor phase current, 10A/div, $I_{rms}=I_n$, f=25Hz, m=0.5, DI sequence; corresponding vector rotation in α-β plane.

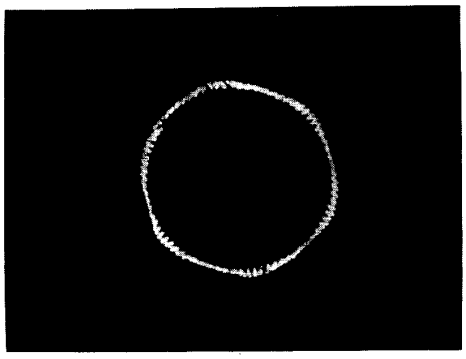

Fig. 8: Motor phase current, 10A/div, $I_{rms}=I_n$, f=50Hz, m=1, DD sequence; corresponding vector rotation in α-β plane.

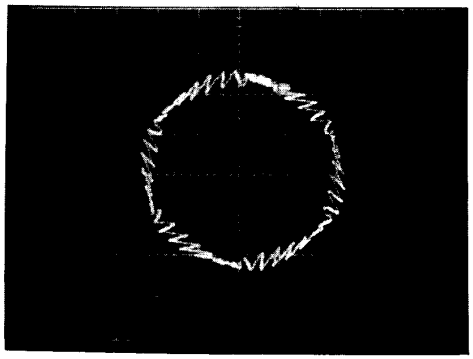

Fig. 9: Motor phase current, 10A/div, $I_{rms}=I_n$, f=50Hz, m=1, DI sequence; corresponding vector rotation in α-β plane.

index m are experimentally verified over a modulation range from 0.2 to 1 by recording the phase current waveforms and then calculating off-line the THD (the THD is the relative value of the ripple RMS value). In order to focus on the difference between DD and DI strategies, the 5-th and 7-th harmonic components as well as the parasitic DC component are excluded from the THD calculations. The results, presented in Fig. 14, are in agreement with those obtained analytically (Fig. 4). Trace B in Fig. 14 represents the RMS value of the current ripple for a DI sequencing. The DI-ripple is larger than the DD-ripple (trace A) for all modulation indexes larger than 0.2. For $m = 1$, the ratio between the DI- and DD-ripple is 2.

The trace C in Fig. 14 shows a projected DI-ripple, derived from trace B by assuming that the cycle frequency is increased by the ratio 4/3. So, traces A and C can serve for a comparison between DD and the DI strategies having the same commutation frequency. The intersection (M) of traces A and C represents the point ($m \approx 0.8$) below which the DI sequence is preferred if one only wants to reduce the commutation frequency and the current ripple.

4. DISCUSSION

For output voltage less than 50% of the rated value and for the same cycle time T, DD and DI space vector modulation strategies give practically the same current spectra, Figs. 10 and 11, and current ripple, Figs. 4 and 14.

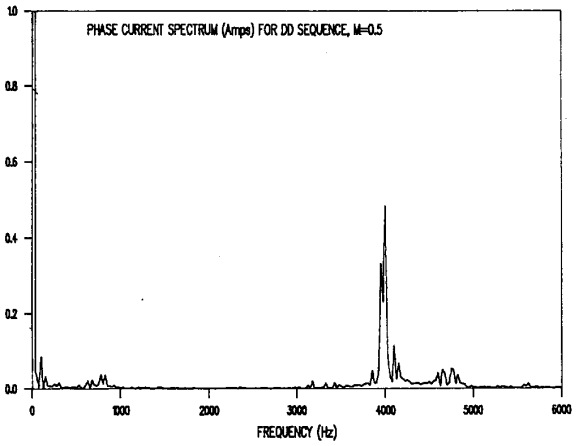

Fig. 10: Spectrum of the phase current shown in Fig. 6.

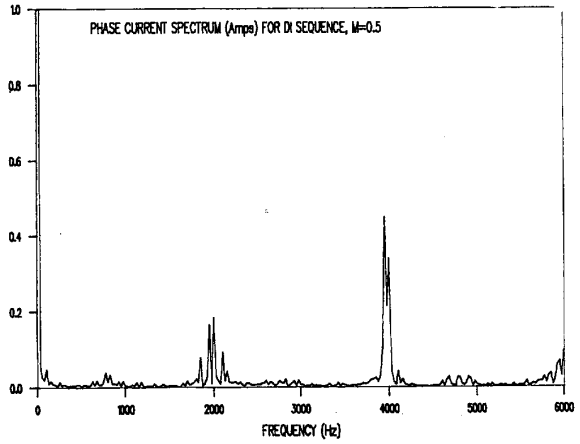

Fig. 11: Spectrum of the phase current shown in Fig. 7.

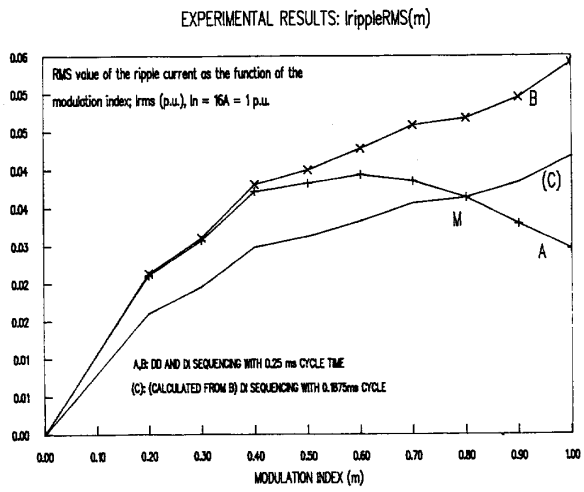

Fig. 14: The RMS value of the current ripple as a function of the modulation index m

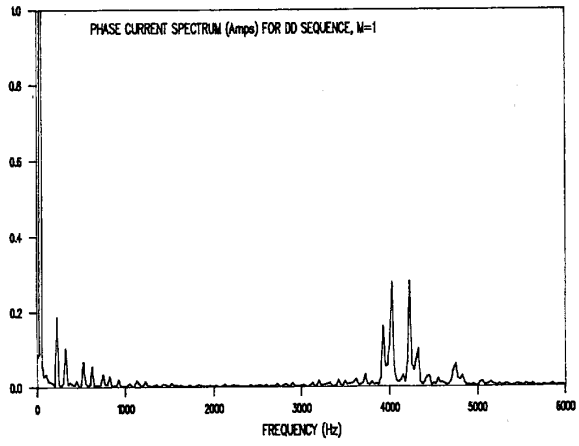

Fig. 12: Spectrum of the phase current shown in Fig. 8.

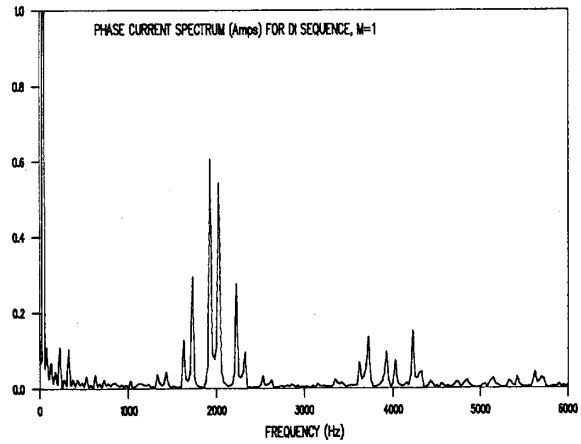

Fig. 13: Spectrum of the phase current shown in Fig. 9.

However, the DI method requires 25% fewer commutations than the DD method.

Above 50% of the rated voltage, the ripple resulting from DI control increases, while that produced by a DD sequence decreases. Specifically, at the full output voltage (m = 1), the DI ripple is twice that produced by the DD control, Figs. 4 and 14. Furthermore, the main ripple component for the DI sequence has migrated to half the cycle frequency, while DD ripple has remained at the cycle frequency, Figs. 12 and 13.

The DI strategy has become popular because it gives three instead of four commutations per cycle. However, one is concerned primarily with the total power loss due to commutations rather than about the number of commutations. For that reason, it is important to analyze the conditions under which the one commutation, eliminated by the DI strategy, occurs. Starting with the expressions for the commutation loss P_γ(DD) (for the DD sequence) and P_γ(DI) (for the DI sequence), calculated in Appendix II and looking at their ratio, $P_\gamma(DD)/P_\gamma(DI)$, given in Table III, one can see the strong influence of the power factor, $\cos(\varphi)$. For typical values of a power factor between 0.75 and 0.92

for an induction motor at a rated load, the reduction in the commutation losses with the DI strategy is less than 1.5%.

TABLE III: Commutation loss for DD and DI sequencing, with the same cycle time, as a function of a lagging power factor

$\cos(\varphi)$	0.0	0.1	0.2	0.3	0.4	0.5
$\frac{P_\gamma(DD)}{P_\gamma(DI)}$	1.49	1.41	1.33	1.26	1.19	1.13

$\cos(\varphi)$	0.6	0.7	0.8	0.9	1.0	-
$\frac{P_\gamma(DD)}{P_\gamma(DI)}$	1.08	1.03	1.01	1.01	1.12	-

For the angle $\varphi = 30^\circ$ ($\cos(\varphi) = 0.866$), the DD- and DI-losses are the same. To understand why the DI sequence does not substantially reduce the commutation loss while reducing the number of commutations, consider sector 1, Fig.1. For $\varphi \cong 30^\circ$, the phase A current in the first sector changes from -30° to 30°, while the phase B current and the phase C currnet lag 120° and 240° respectively. Hence, ia goes through its maximum in sector 1, while ib and ic go through zero. Therefore, it can be expected that tha average values of $|ib|$ and $|ic|$ will be significantly lower than the average $|ia|$ in the first sector. So, the DI sequence is replacing four "low-current commutations" of the DD sequence (2B+2C, Fig. 2) with one "high -current" commutation and two "low-current" commutations (A + B + C, Fig. 3). For that reason, the ratio $P\gamma(DD)/P\gamma(DI)$ is close to 1 (Table III) for $\cos(\varphi) \in 0.7..0.9$. On the other hand, if the load is purely inductive, the ratio will be 1.5 according to Table III; that is, the commutation losses will be significantly reduced if the DI strategy is applied.

For cases of AC drives during motoring and for UPS systems, the ratio $P\gamma(DD)/P\gamma(DI)$ will be close to 1 under the rated load conditions. Different values of the $\cos(\varphi)$ and the ratio $P\gamma(DD)/P\gamma(DI)$ can be expected for no-load conditions, where the current amplitude and the commutation losses are anyhow low. Therefore, in most applications the DI sequence will produce the commutation losses similar to the losses of the DD sequence, regardless of the 25% reduction in the number of commutations. This means that curves A and B, Fig. 4, have approximately the same commutation losses. Considering now the ripple, Fig. 4, it is clear that one should select the regular (DD) sequence (curve A) over the entire operating range.

If the angle φ of the inverter load varies in a wide range (or cannot be defined), the DI sequencing may result in a significant reduction of the commutation loss (in Table III, $P\gamma(DD)/P\gamma(DI) = 1.5$ for inductive loads, $\cos(\varphi) = 0$). At the same time, the DI sequence results in an increased current ripple, curve B, Fig. 4. Assuming for a moment that the commutation losses depend only on the number of commutations and not on conditions during commutation (sequence DD or DI), one would switch from a DI to a DD sequence above $m = 0.75$, Fig. 4. In principle, the DI commutations will always be more "lossy" than DD commutations so that a switch-over point M will be at values of the modulation index lower than shown in Fig. 4. The exact calculation of the switch-over point requires knowledge of the commutation loss, which, in turn, depends on the load, the load power factor, the type of power switches and the snubber circuit. In summary, the DD sequence should be used with standard industrial motor drives. For other loads, one should consider the DI sequence for low output voltages and the DD sequence when the modulation index is high. The exact switch-over from one to the other sequence will depend on the commutation losses.

The DI sequence should never be used for high output voltages, due to a significant increase in the current ripple.

5. CONCLUSION

Characteristics of regular (DD) and inverted (DI) sequencing strategies are investigated both analytically and experimentally. The two strategies are compared with respect to the current ripple, the current spectrum, and the commutation losses. It was found that DD sequence offers superior performance for majority of loads such as induction motor drives. For other types of inverter loads, with small or leading power factors, the optimal modulation strategy consists in using the DI sequence when the output voltage is low, and the DD sequence if the modulation index is between m(M) and 1. For best results, the switch-over point M has to be evaluated in function of load and inverter design.

REFERENCES:

[1] A. Busse, J. Holtz: "A digital space vector modulator for the control of a three-phase power converter", *in VDE -Konferenz Mikroelektronik in Stromrichtertechnik und bei elektrischen Antrieben,* Darmstadt, November 1982, pp 189-195

[2] A.J. Pollman: "Software Pulsewidth Modulation for Microprocessor Control of AC Drives", *IEEE Trans. Ind. Appl.*, **vol. IA-22**, No. 4, pp 691-696, July/Aug. 1986.

[3] J. Holtz, P. Lammert, and W. Lotzkat: "High-Speed Drive System with Ultrasonic MOSFET PWM Inverter and Single-Chip Microprocessor Control", *IEEE Trans. Ind. Appl.*, **vol. IA-23**, No. 6, pp 1010-1015, Nov/Dec. 1987.

[4] H.W. van der Broeck, H.C.Skudelny, G.V. Stanke: "Analyses and Realization of a Pulsewidth Modulator Based on Voltage Space Vectors", *IEEE Trans. Ind. Appl.*, **vol. IA-24**, No. 1, pp 142-150, Jan/Feb. 1988.

[5] Heinz Willi van der Broeck: "Vergleich von spannungseinpragenden Wechselrichtern mit zwei und drei Zweigpaaren zur Speisung einer Drehstromasynchronmaschine unter Verwedung der Pulsweitenmodulation hoher Taktzahl", Dissertation, Rheinisch -Westfalische Technische Hochschule, Aachen, 1985.

[6] P.D. Ziogas et al: "A refined PWM scheme for Voltage and Current Source Inverters", *in Conf. Rec. of the 1990. IEEE IAS Annual Meeting,* pp 977-983.

APPENDIX I
CALCULATION OF THE RMS RIPPLE CURRENT AS A FUNCTION OF THE MODULATION INDEX m

DD sequencing strategy:

Neglecting the stator resistance and assuming that the switching cycle T is essentially small with respect to the motor dynamics, one concludes that the motor current will change linearly between the two commutation instants. Referring to Fig. 2 and considering the reference vector at $\Delta\theta = 30^{\circ}$ (where the current ripple is maximum), the time intervals and the average α and β voltage components within the switching cycle T are:

$$t_1 = \frac{mT}{2}\ , \quad t_2 = mT\ , \quad T_1 = T_2 = \frac{mT}{2}\ ; \tag{A1}$$

$$U_{\alpha}^{av} = \frac{3}{4}\,mE\ , \quad U_{\beta}^{av} = \sqrt{3}\,\frac{mE}{4}. \tag{A2}$$

Under the assumption that the back EMF induced in the stator windings is balanced by the inverter output voltage, the current ripple can be calculated as the current flowing through the equivalent leakage inductance of the motor exposed to the difference between the voltage reference and the inverter instantaneous output. The α and β components of the stator current at the instants $t0..t3$ (Fig.2) can be calculated as:

$$i_{\alpha}(t_0) = I_{\alpha 0},\ i_{\beta}(t_0) = I_{\beta 0} \text{ (initial values)} \tag{A3}$$

$$i_{\alpha}(t_1) = I_{\alpha 0} + \left(E - \frac{3mE}{4}\right)\frac{mT}{2L_{\sigma}}\ , \tag{A4}$$

$$i_{\beta}(t_1) = I_{\beta 0} - \sqrt{3}\,\frac{mE}{4}\,\frac{mT}{2L_{\sigma}}\ .$$

$$i_{\alpha}(t_2) = I_{\alpha 0} + \frac{3}{2}\,E(1-m)\,\frac{mT}{2L_{\sigma}}\ , \tag{A5}$$

$$i_{\beta}(t_2) = I_{\beta 0} + \sqrt{3}\,\frac{E(1-m)}{2}\,\frac{mT}{2L_{\sigma}}$$

$$i_{\alpha}(t_3) = I_{\alpha 0},\quad i_{\beta}(t_3) = I_{\beta 0} \tag{A6}$$

$$i_{\alpha}^{av}(t_0..t_3) = I_{\alpha 0} + \frac{m}{2}i_{\alpha}(t_1) + \tag{A7}$$

$$+ \left(\frac{1}{2} - \frac{m}{4}\right)i_{\alpha}(t_2) = \frac{mTE}{2L_{\sigma}}\,\frac{6-5m}{8} + I_{\alpha 0}.$$

$$i_{\beta}^{av}(t_0..t_3) = I_{\beta 0} + \frac{m}{2}i_{\beta}(t_1) + \tag{A8}$$

$$+ \left(\frac{1}{2} - \frac{m}{4}\right)i_{\beta}(t_2) = \frac{mTE}{2L_{\sigma}}\,\sqrt{3}\,\frac{2-3m}{8} + I_{\beta 0}.$$

From A3-A8, and assuming the linear change of the current between the switching instants, the RMS value of the α- and β-ripple components are found as:

$$\Delta i_{\alpha rms}^2 = \frac{1}{T}\int_{t_0}^{t_3} i_{\alpha}^2(t)dt - (i_{\alpha}^{av})^2 \tag{A9}$$

$$\Delta i_{\beta rms}^2 = \frac{1}{T}\int_{t_0}^{t_3} i_{\beta}^2(t)dt - (i_{\beta}^{av})^2 \tag{A10}$$

$$\Delta i_{\alpha\beta rms}^2 = \left(\frac{mTE}{2L_{\sigma}}\right)^2\left(\frac{1}{4} - \frac{5m}{12} + \frac{3m^2}{16}\right). \tag{A11}$$

DI sequencing strategy:

From Fig.3, it is clear that the ripple waveform (under the same assumptions as above) will be a periodic function with a period $2T$. Hence, it is necessary to calculate the current values from $t3$ to $t6$:

$$i_{\alpha}(t_4) = I_{\alpha 0} + \left(\frac{E}{2} - \frac{3m}{4}\right)\frac{mTE}{2L_{\sigma}}, \tag{A12}$$

$$i_{\beta}(t_4) = I_{\beta 0} + \frac{\sqrt{3}}{2}\,\frac{mTE}{2L_{\sigma}}\left(1 - \frac{m}{2}\right).$$

$$\vec{I}_{\alpha\beta}(t_5) = \vec{I}_{\alpha\beta}(t_2), \tag{A13}$$

$$\vec{I}_{\alpha\beta}(t_0) = \vec{I}_{\alpha\beta}(t_3) = \vec{I}_{\alpha\beta}(t_6) = [I_{\alpha 0}, I_{\beta 0}]$$

The average values of α and β current components in the interval $[t0..t6]$ of the DI sequence (Fig.3) can be calculated as in (A7-A8), and are found to be:

$$i_{\alpha}^{av}(t_0..t_6) = \frac{mTE}{2L_{\sigma}}\,\frac{3}{4}(1-m) + I_{\alpha 0}\ , \tag{A14}$$

$$i_{\beta}^{av}(t_0..t_6) = \frac{\sqrt{3}}{4}\,\frac{mTE}{2L_{\sigma}}\,(1-m).$$

The RMS values of the α and β ripple components for the DI interval $[t0..t6]$ are given by (A15-A16).

$$\Delta i_{\alpha rms}^2 = \frac{1}{2T}\int_{t_0}^{t_6} i_{\alpha}^2(t)dt - (i_{\alpha}^{av})^2 \tag{A15}$$

$$\Delta i_{\beta rms}^2 = \frac{1}{2T}\int_{t_0}^{t_6} i_{\beta}^2(t)dt - (i_{\beta}^{av})^2 \tag{A16}$$

The total ripple RMS value for the DI sequence, is given by (A17).

$$\Delta i_{\alpha\beta rms}^2 = \left(\frac{mTE}{2L_{\sigma}}\right)^2\left(\frac{1}{4} - \frac{5m}{12} + \frac{m^2}{4}\right). \tag{A17}$$

APPENDIX II
Comparison of the DD and DI sequences with respect to the commutation losses for different values of the load angle φ

One cycle of DI space vector modulation (Fig.3) comprises one transition of each inverter leg (the total of 3; A,B,C). In the case of DD strategy, the total number of transitions is 4, and within each 60° wide sector, one of the inverter legs is not commutating. Introducing Nx as the number of commutations in phase "x" during one cycle, the DI and DD transitions in the first sector (Fig.1) can be described as:

$$N_a(DD) = 0,\quad N_b(DD) = 2,\quad N_c(DD) = 2 \tag{A18}$$

$$N_a(DI) = 1,\quad N_b(DI) = 1,\quad N_c(DI) = 1 \tag{A19}$$

The energy loss per one commutation can be considered roughly proportional to the current which is commutated, $\Delta W = Kw\ i$. If the cycle frequency is $fc = 1/T$, the average power losses $P\gamma$ due to the bridge commutations can be expressed as:

$$P_{\gamma} = K_w\ f_c(N_a|i_a|_{av} + N_b|i_b|_{av} + N_c|i_c|_{av}) \tag{A20}$$

The comparison of the DD and DI space vector modulation with respect to the commutation losses is done on the relative basis; that is, the ratio between $P\gamma(DD)$ and $P\gamma(DI)$ is calculated for different values of the load angle φ. The results are given in the Table III, for inductive loads and $\cos(\varphi)$ range 0-1.